

**$\alpha$ -clustering folding model**

M. El-Azab Farid, Z. M. M. Mahmoud, and G. S. Hassan

*Physics Department, Assiut University, Assiut 71516, Egypt*

(Received 18 July 2000; published 8 June 2001)

$\alpha$ -nucleus single-folding cluster optical potentials based upon the  $\alpha$ -cluster model and an  $\alpha$ - $\alpha$  interaction were generated for  $m\alpha$ -cluster structure targets ( $m=3, 4, 6, 7,$  and  $8$ ). Angular distributions of the differential cross section of  $\alpha$  elastic scattering by  $^{12}\text{C}$ ,  $^{16}\text{O}$ , and  $^{28}\text{Si}$  have been analyzed for various incident energies using the derived potentials. Also, single-folding optical model potentials were constructed using an  $\alpha$ -nucleon effective interaction to analyze the same data. Both models produced reasonable success in predicting scattering data, particularly at higher energies. The effect of uncertainties in the projectile and target nuclear densities on the results was investigated. The energy dependence of the calculated potentials is also discussed.

DOI: 10.1103/PhysRevC.64.014310

PACS number(s): 21.60.Gx, 24.10.Ht, 25.60.Bx, 25.70.-z

**I. INTRODUCTION**

The scattering of an  $\alpha$ -particle projectile from light heavy-ion nuclei has been of special interest because elastic scattering cross sections exhibit two different features. The first is usually known as anomalous large angle scattering (ALAS) [1], where an unusual enhancement of cross section is observed at back angles. This phenomenon is clearly manifested in scattering from doubly closed shell light nuclei, e.g.,  $^{16}\text{O}$  and  $^{40}\text{Ca}$ . The enhancement of back angle scattering decreases as the energy of the  $\alpha$  particle increases but the whole effect disappears for energies above 55 MeV for all target nuclei.

The second feature is nuclear rainbow scattering [2], which is observed for  $\alpha$  energies above 100 MeV characterized by a sharp decrease of cross section beyond a certain scattering angle, known as the grazing angle. This phenomenon can be used to probe the nucleus-nucleus potential, not only in the surface region but also at smaller distances and could be of considerable practical use in eliminating certain potential ambiguities that arise in the analysis of elastic scattering data. Within the framework of simple scattering theory, deeper insight is provided by deconvoluting the elastic scattering amplitude into two components corresponding to scattering from the nearside and farside of the target.

The interpretation of these two features has played a decisive role in establishing a unique  $\alpha$ -nucleus optical potential [1]. It was found that the ‘‘usual’’ Woods-Saxon (WS) type of optical potentials is inadequate to analyze large angle elastic  $\alpha$  scattering from light- and medium-weight nuclei. Therefore, to investigate the ALAS phenomenon, some have used arbitrary  $(\text{WS})^n$  ( $n > 2$ ) form factors [3]. Michel *et al.* [4] suggested a flexible parametrization of the real part of the optical potential. This produced a radial variation as well as an energy dependence for the best fit real potential exhibiting a good accuracy for  $\alpha$  scattering from  $^{16}\text{O}$  over a wide range of energies.

Also, the real part of the optical potential calculated using the double-folding model yielded a good account of  $\alpha$  scattering over a wide range of energies and target mass numbers [5,6]. This points out the ability of the folding concept to predict the radial shape of real potentials.

On the other hand, there are many lines of evidence that

nucleons inside the nucleus tend to form clusters [7], and the most likely form of these clusters is the  $\alpha$  particle because of its symmetry and high binding energy (28.3 MeV). Near the nuclear surface, where the nuclear density falls rapidly to zero, alpha clusters become more stable. Since the  $\alpha$ -target interaction mainly takes place near the nuclear surface, the  $\alpha$  correlation should be the strongest and the  $\alpha$  cluster is expected to behave in many respects like a free  $\alpha$  particle. The form of an  $\alpha$  cluster can be used to explain the ALAS behavior, where the enhancement of cross sections at backward angles is suggested to be related to the presence of an  $\alpha$  correlation in the ground state of target nuclei [8]. Therefore, the  $\alpha$ -cluster model has been employed to calculate folded optical model potentials for composite projectiles through either the Watanabe superposition model [9] or the single-folding cluster (SFC) [8] and double-folding cluster [10–12] models.

In the present work we derived  $m\alpha$ -cluster densities for  $^{12}\text{C}$ ,  $^{16}\text{O}$ ,  $^{24}\text{Mg}$ ,  $^{28}\text{Si}$ , and  $^{32}\text{S}$  nuclei to generate the  $\alpha$ -nucleus optical potentials through the SFC model. The resulting potentials were employed to analyze elastic scattering data for  $\alpha + (^{12}\text{C}, ^{16}\text{O}, \text{ and } ^{28}\text{Si})$  systems in the range  $E = 18.5\text{--}172$  MeV laboratory energy. Furthermore, for convenience, we folded an  $\alpha$ -nucleon ( $\alpha$ - $n$ ) interaction over the ground-state nuclear density of the target nucleus to obtain the single-folding matter (SFM) optical potentials that were used to analyze the same data.

**II. THEORETICAL FORMALISM**

Consider a nucleus of mass number  $A$  composed of an integral number ( $m$ ) of  $\alpha$  particles, i.e.,  $A = 4m$ . If the  $\alpha$ -cluster distribution function inside the nucleus is  $\rho_C(r')$ , we relate the nuclear matter density distribution function of the nucleus,  $\rho_M(r)$ , to that of the  $\alpha$ -particle nucleus,  $\rho_\alpha(r)$ , as

$$\rho_M(r) = \int \rho_C(r') \rho_\alpha(|\vec{r} - \vec{r}'|) d\vec{r}'. \quad (1)$$

In our calculation we use a modified Gaussian form for the target density  $\rho_M(r)$  and a Gaussian form for the  $\alpha$ -particle density  $\rho_\alpha(r)$  as follows:

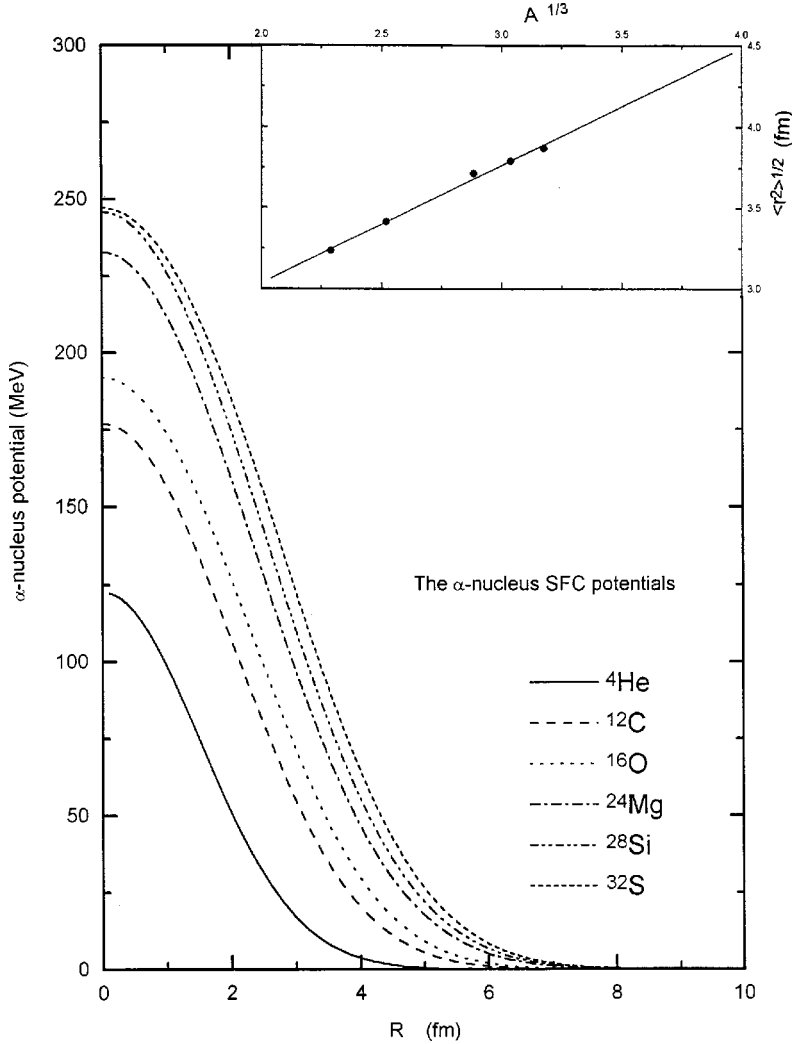


FIG. 1. The obtained  $\alpha$ -nucleus single-folding cluster (SFC) potentials. The inset shows the root-mean-square radii of the calculated SFC potentials versus  $A^{1/3}$ .

$$\rho_M(r) = \rho_{0M}(1 + \omega r^2)\exp[-\beta r^2], \quad (2)$$

$$\rho_\alpha(r) = \rho_{0\alpha}\exp[-\lambda r^2], \quad (3)$$

where the parameters  $\omega$ ,  $\beta$ , and  $\lambda$  are taken from Refs. [13–19].  $\rho_{0\alpha}$  and  $\rho_{0M}$  can be determined from the normalization condition

$$\int \rho(r)r^2 dr = \frac{A}{4\pi}. \quad (4)$$

To calculate the  $\alpha$ -cluster distribution function  $\rho_C(r')$  from expression (2) we use Fourier transform techniques [13].

In order to generate the real part of the  $\alpha$ -nucleus optical potential one may apply the double-folding (DF) concept based upon the matter densities of both the  $\alpha$ -particle and target nuclei and a suitable effective  $NN$  interaction. However, here, we use two semimicroscopic approaches to construct the real part of the optical potential. For the first approach, we derive the SFM  $\alpha$ -nucleus potential by folding an effective  $\alpha$ - $n$  interaction [20] with the nuclear matter density of Eq. (2). We use the  $\alpha$ - $n$  interaction in the form of a Gaussian shape [20]. For the second approach, we build the SFC

potential based upon an  $\alpha$ - $\alpha$  interaction folded over the  $\alpha$ -cluster distribution function of the target nucleus.

The  $\alpha$ - $\alpha$  system has been investigated by several theoretical and experimental studies. At least three different approaches have been performed to analyze low energy  $\alpha$ - $\alpha$  elastic scattering data using a purely attractive local angular momentum and energy independent  $\alpha$ - $\alpha$  potential [21–23]. Some other studies [24,25] used a phenomenological  $\alpha$ - $\alpha$  potential including a short-range repulsive and a long-range attractive part. Satchler and Love [13] calculated an  $\alpha$ - $\alpha$  DF potential based on the M3Y effective interaction involving an exchange contribution for energy 10 MeV per nucleon. The resulting potential, which is also purely attractive, is very similar to that of Buck, Friedrich, and Wheathly [22]. Therefore, we found that the  $\alpha$ - $\alpha$  potential of Buck, Friedrich, and Wheathly [22] is the most favorable and the simplest one to be considered in our calculation.

For both SFM and SFC procedures, the  $\alpha$ -nucleus folded potential is derived from the expression

$$V_{\text{SFi}}(R) = \int \rho_i(r)V_{\alpha j}(|\vec{R} - \vec{r}|)d\vec{r}, \quad (5)$$

TABLE I. The obtained SFC optical model potential parameters, volume integrals, total reaction cross sections  $\sigma_R$ , and  $\chi^2$  values.

$E$ (MeV)	$N_r$	$W_0$ (MeV)	$r_W$ (fm)	$a_W$ (fm)	$-J_I$ (MeV fm <sup>3</sup> )	$\chi^2$	$\sigma_R$ (mb)
$\alpha + {}^{12}\text{C}$							
18.5	1.90	14.500	0.7500	0.350	9.04	798.0	744.2
28.4	1.07	12.157	1.4932	0.090	42.67	1690.0	806.9
41.0	1.05	45.540	1.2400	0.650	138.04	190.9	912.1
48.7	0.93	65.160	1.2664	0.455	172.28	322.0	767.1
54.1	0.89	76.540	1.2460	0.450	193.14	151.6	742.8
104.0	0.61	33.421	0.8270	1.144	94.98	7.54	884.0
120.0	0.61	10.545	1.8396	0.803	93.23	8.03	854.6
139.0	0.71	15.443	1.8030	0.492	108.08	19.3	719.1
166.0	0.51	5.961	2.3240	0.616	88.67	3.12	813.3
172.5	0.48	4.611	2.6230	0.609	95.87	2.16	907.0
$\alpha + {}^{16}\text{O}$							
32.2	0.87	14.50	1.152	0.63	34.02	353.8	881.2
40.4	0.88	12.45	1.356	0.68	45.21	93.3	902.1
48.7	0.86	16.20	1.365	0.79	65.58	43.0	978.5
54.1	0.85	16.30	1.394	0.77	68.14	12.62	960.0
65.0	0.82	16.55	1.573	0.78	93.13	8.07	1047.0
80.7	0.80	16.15	1.579	0.61	82.02	9.58	875.8
104	0.76	16.95	1.595	0.60	87.86	5.37	843.8
146	0.71	16.21	1.701	0.73	107.36	17.95	947.8
$\alpha + {}^{28}\text{Si}$							
104.	0.87	37.1	1.365	0.79	134.03	8.44	1285.0
166	0.62	18.25	1.55	0.61	82.94	3.26	1013.0

where  $i = M, j = n$  for the first procedure and  $i = C, j = \alpha$  for the second one.

### III. PROCEDURE

We calculated the SFM and SFC potentials for  $\alpha + ({}^{12}\text{C}, {}^{16}\text{O}, {}^{24}\text{Mg}, {}^{28}\text{Si}, \text{ and } {}^{32}\text{S})$  systems ( $m = 3, 4, 6, 7,$  and  $8$ ) to be used as the real part of  $\alpha$ -nucleus optical potentials. We have chosen three of the calculated interactions,  $\alpha + ({}^{12}\text{C}, {}^{16}\text{O}, \text{ and } {}^{28}\text{Si})$ , to analyze several sets of elastic scattering data in a wide range of energies. The imaginary parts of the  $\alpha$ -nucleus optical potential were parametrized phenomenologically in a WS shape. Elastic scattering cross section calculations were carried out using the computer code HIOPTIM-94 [26]. We used the average error for all considered sets of data to be 10%. The searches were carried out by optimizing four free parameters, a real renormalization factor  $N_r$  for the calculated potentials besides the three parameters of the imaginary phenomenological WS potential.

### IV. RESULTS AND DISCUSSION

The obtained  $\alpha$ -cluster distribution densities were used to calculate the  $\alpha$ -nucleus SFC potentials (5) for  ${}^{12}\text{C}, {}^{16}\text{O}, {}^{24}\text{Mg}, {}^{28}\text{Si}, \text{ and } {}^{32}\text{S}$  targets. The resulted potentials are shown in Fig. 1. It is obvious that the depth of the interaction increases as the mass number increases. The rms radii of the

TABLE II. Same as Table I but for the SFM optical potential.

$E$ (MeV)	$N_r$	$W_0$ (MeV)	$r_W$ (fm)	$a_W$ (fm)	$-J_i$ (MeV fm <sup>3</sup> )	$\chi^2$	$\sigma_R$ (mb)
$\alpha + {}^{12}\text{C}$							
18.5	1.25	14.500	0.7500	0.370	9.350	1017.0	783.2
28.4	0.77	11.802	1.1610	0.732	33.90	2355.0	761.9
41.0	1.15	45.540	1.2400	0.650	138.04	188.6	933.1
48.7	0.95	53.160	1.2554	0.500	143.05	296.2	778.8
54.1	0.90	75.540	1.2460	0.450	190.61	91.65	737.3
104.0	0.84	25.279	1.3140	0.846	107.00	3.19	841.0
120.0	0.938	14.244	1.8786	0.541	114.32	5.18	814.7
139.0	0.89	14.691	1.8840	0.491	116.03	5.34	770.1
166.0	0.84	13.457	1.8860	0.574	111.02	4.01	769.4
172.5	0.68	25.722	0.9470	1.289	105.40	1.50	894.8
$\alpha + {}^{16}\text{O}$							
32.2	1.03	15.00	1.141	0.70	37.01	205.0	952.2
40.4	1.00	12.51	1.365	0.67	45.79	71.53	915.8
48.7	1.00	16.59	1.353	0.82	67.55	53.52	1012.0
54.1	0.98	16.50	1.394	0.80	70.72	11.31	996.5
65	0.95	17.30	1.577	0.82	100.73	7.00	1105.0
80.7	0.92	16.10	1.588	0.65	85.08	5.70	916.9
104	0.87	16.20	1.599	0.70	89.98	3.94	913.1
146	0.80	15.75	1.700	0.83	110.77	8.33	1021.0
$\alpha + {}^{28}\text{Si}$							
104	0.97	37.1	1.365	0.79	134.03	8.86	1280.0
166	0.75	18.75	1.55	0.64	86.42	3.76	1049.0

derived SFC potentials are plotted against the cube root of  $A$ , as seen in the inset in Fig. 1. We notice that, the rms radius has a clear linear dependence on  $A^{1/3}$ . This linearity can be represented as

$$\langle r^2 \rangle^{1/2} = 1.38[1 + 0.58A^{1/3}]. \quad (6)$$

From this relation, it is easy to interpolate the corresponding rms radius for the  ${}^{20}\text{Ne}$  nucleus or to extrapolate those of the other  $m\alpha$ -cluster structure nuclei such as  ${}^{36}\text{Ar}, {}^{40}\text{Ca}, \text{ and } {}^{44}\text{Ti}$  nuclei.

On the other side, our calculated potentials are consistent with those obtained by Friedrich and Langanke [27] and with Buck, Merchant, and Perez [28] considering the  $\alpha$ -cluster structure of  ${}^{16}\text{O}$ . However, the obtained normalized  $\alpha + {}^{16}\text{O}$  potentials are deeper than those derived by Yamaguchi, Yabana, and Hariuchi [29]. Nevertheless, those potentials [29] have an energy dependence similar to that obtained in the present work.

We analyzed 27 sets of data for the angular distribution differential cross sections of the of  $\alpha$ -particle elastic scattering from  ${}^{12}\text{C}, {}^{16}\text{O}, \text{ and } {}^{28}\text{Si}$  targets using the calculated SFC and SFM potentials. The obtained best fit values of the real normalization factor  $N_r$  and imaginary potential parameters are listed in Tables I and II, respectively. The predicted elastic scattering cross sections are shown in comparison with experimental data in Figs. 2–6. A general look at these figures shows that the two (SFC and SFM) potentials produce almost similar elastic scattering predictions. The two interac-

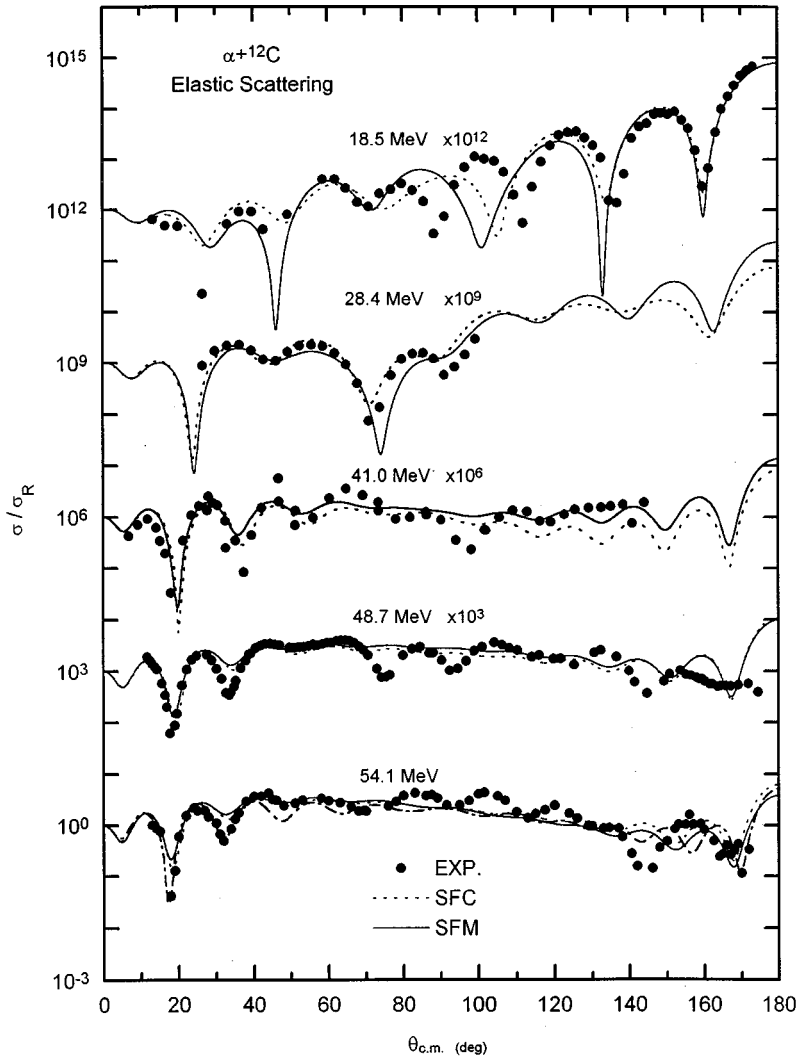


FIG. 2. Angular distributions for the elastic scattering of  $\alpha$  particles from  $^{12}\text{C}$  obtained by SFC and SFM potentials in comparison with experimental data at energies 18.5 [20], 28.4 [31], 41 [32], 48.7, and 54.1 [6] MeV.

tions,  $\alpha$ - $\alpha$  and  $\alpha$ - $n$  (on which the SFC and SFM potentials, respectively, are built), were separately parametrized [22,20]. This indicates that the SFC potentials are as realistic or semi-realistic as the SFM potentials. In other words, the presented SFC model is as successful as the semimicroscopic SFM one.

### A. $\alpha + ^{12}\text{C}$ system

The elastic cross sections of  $\alpha$  particles scattered from  $^{12}\text{C}$  have been measured over a wide range of energies,  $E = 18.5$ – $172.5$  MeV. We divide this range into two categories. We consider five data sets below 55 MeV (18.5, 28.4, 41, 48.7, and 54.1 MeV) where the ALAS phenomenon can be investigated. The other five data sets are above 100 MeV (104, 120, 139, 166, and 172 MeV) where rainbow scattering is apparent.

For the 18.5-MeV reaction, as shown in Fig. 2, both SFC and SFM potentials produce similar qualitative fits to the data for forward and backward angles, however, there is a phase shift between the calculated and measured cross sections around  $\theta_{\text{c.m.}} = 100^\circ$ . Baz *et al.* [30] analyzed these data using a phenomenological optical potential. They have ob-

tained successful predictions only when they introduced a hard core potential ( $R_{\text{core}} \sim 2.72$  fm) to take into account the effect of the Pauli principle, which plays an important role at low energies. It is obvious also that the SFC and SFM potentials describe the ALAS region successfully. At  $E = 28.4$  MeV [31], the SFC potential describes the data quite well up to  $\theta_{\text{c.m.}} = 100^\circ$ , while the SFM predictions are not so successful for  $\theta_{\text{c.m.}} > 80^\circ$ . The two models qualitatively reproduced the data at  $E = 41$  MeV up to  $\theta_{\text{c.m.}} = 140^\circ$  and their fits are comparable to that obtained using the phenomenological WS potential suggested by Baron, Leonard, and Stewart [32].

For  $E = 48.7$  and 54.1 MeV data, our predictions are similar to those resulting from the real DF potentials derived by Abele *et al.* [6] using the DDM3Y  $NN$  interaction, where the imaginary potential was expressed in terms of a Fourier-Bessel function of six terms, and by Khallaf, Amry, and Mokhtar [33] (for 54.1 MeV only) using the JLM  $NN$  interaction. The discrepancy between observed and calculated cross sections is attributed to the strong deformation of the carbon nucleus in its ground state. Therefore, they [6] recommended using the coupled channel method to analyze these data, i.e., at these energies, elastic scattering channels

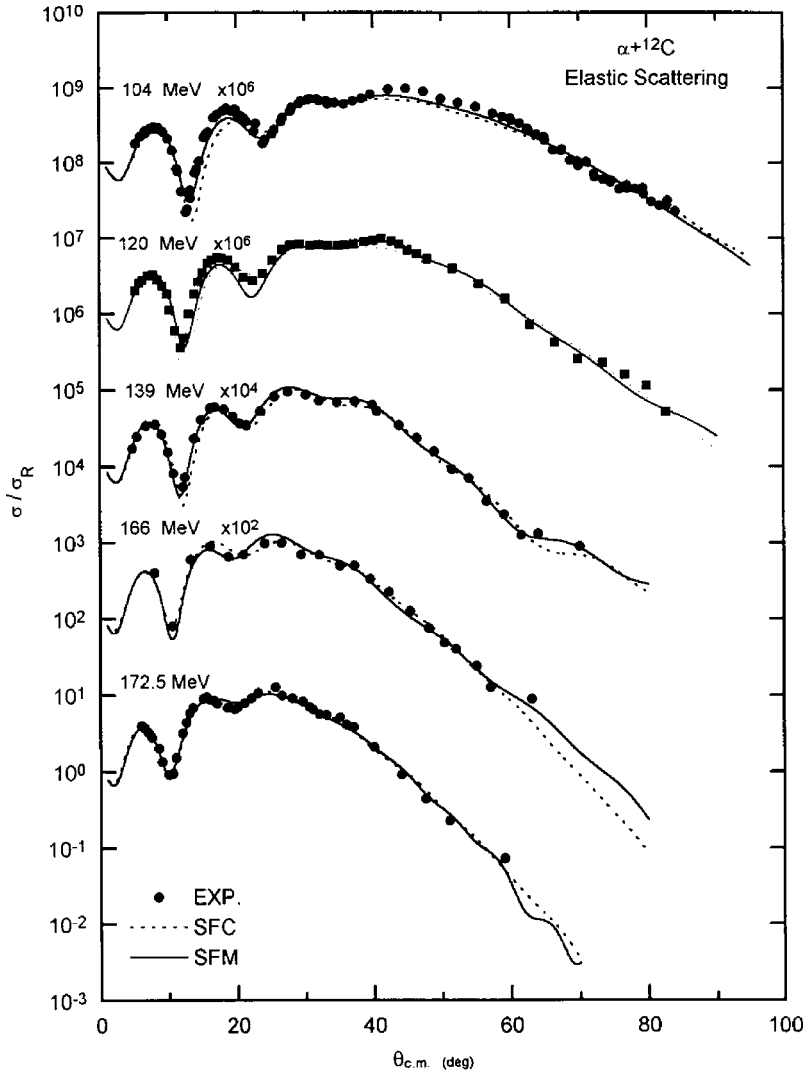


FIG. 3. Same as Fig. 2 but at energies 104 [35], 120 [36], 139 [34], 166, and 172.5 [39] MeV.

are strongly coupled to the nonelastic scattering ones. The predictions of the phenomenological potential [6] are shown in a dot-dashed line in Fig. 3 for the 54.1-MeV data. It is clear that SFC and SFM predictions are more successful than those of the phenomenological potential [6].

Results for reactions at  $E > 100$  MeV are shown in Fig. 3. It is clear that SFC and SFM potentials yielded successful predictions for the data at  $E = 104, 120, 139, 166,$  and  $172.5$  MeV. Our fits are quite satisfactory as those obtained using phenomenological optical potentials [34–39] and also those using microscopic DF potentials built upon Gaussian [40,41] M3Y [2], and JLM [33]  $NN$  interactions. We notice from Table I that best fits to data are obtained with  $N_r = 1 \pm 0.07$  for the SFC potential at energies 28.5, 41.0, and 48.7 MeV. However, as the energy goes down close to the Coulomb barrier the required  $N_r$  factor increases up to 1.9. This is a similar result to that previously obtained for DF potentials based upon M3Y [13] and DDM3Y [42]  $NN$  interactions. As the energy increases higher than 50 MeV,  $N_r$  values for the SFC potential decrease. Similar behavior can be seen for SFM potential results. Excluding results at 18.5 MeV, the energy dependence of  $N_r$  values for both potentials can be described by the least-squares lines

$$N_r^{\text{SFC}} = 1.14[1 - 0.0034E], \quad (7)$$

$$N_r^{\text{SFM}} = 1.00[1 - 0.0011E]. \quad (8)$$

The energy dependence of the SFM renormalization factor is weaker than that of the SFC renormalization and they have the same value, 0.95, at  $E = 50$  MeV.

### B. $\alpha + {}^{16}\text{O}$ system

Figure 4 shows the resulting elastic scattering cross sections for the  $\alpha + {}^{16}\text{O}$  reaction at eight energies starting from 32.2 MeV up to 146 MeV using the calculated SFM and SFC potentials. It is clear that both potentials produce similar successful predictions for both the ALAS and the rainbow regions. The SFM potential produces more successful predictions than SFC at 40.4 MeV around  $\theta_{\text{c.m.}} = 100^\circ$  and for 54.1 MeV around  $\theta_{\text{c.m.}} = 20^\circ$ . For the 54.1-MeV data, our fits to data are indistinguishable from the phenomenological potential predictions as shown in Fig. 4.

Michel *et al.* [4] have measured the  $\alpha + {}^{16}\text{O}$  elastic scattering angular distributions at the backward angles  $\theta_{\text{c.m.}} = 120^\circ - 180^\circ$  for seven energies in the range 40–54 MeV.

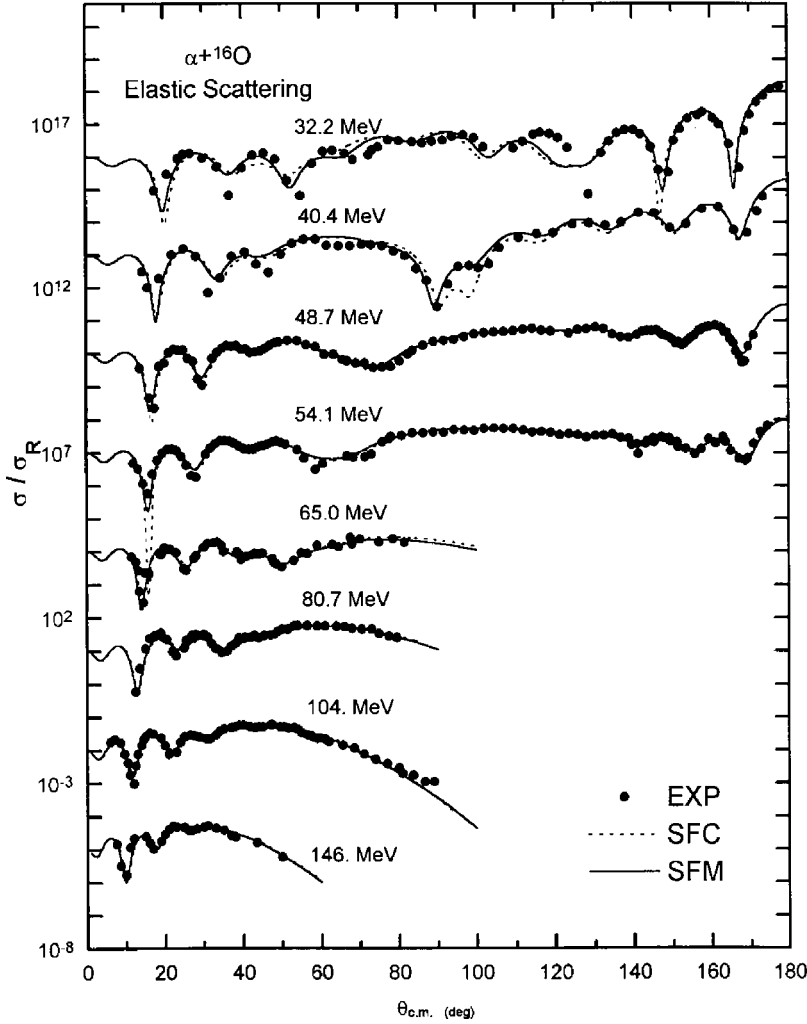


FIG. 4. Same as Fig. 2 but for  $^{16}\text{O}$  target at energies 32.2 [5], 40.4 [5], 48.7 [6], 54.1 [6], 65 [44], 80.7 [5], 104 [35], and 146 [5] MeV.

They analyzed these data using a global phenomenological optical potential with two energy-dependent parameters. In this work we analyzed these seven sets of data using both the SFC and SFM potentials. The resulting cross sections are shown in comparison with data in Fig. 5. It is clear that both potentials produce successful predictions for the data.

A clear energy-dependence tendency is noticed for  $N_r$  of the  $\alpha + ^{16}\text{O}$  system as

$$N_r^{\text{SFC}} = 0.93[1 - 0.0017E], \quad (9)$$

$$N_r^{\text{SFM}} = 1.09[1 - 0.0019E]. \quad (10)$$

It is clear that both the SFC and SFM potentials show a similar energy dependence, but  $N_r^{\text{SFM}}$  values are slightly higher than those of  $N_r^{\text{SFC}}$ .

On the other hand, our fits shown in Fig. 4 are quite similar to those obtained by the DF potentials built upon DDM3Y and JLM  $NN$  effective interactions by Abele *et al.* [6] and Khallaf, Amry, and Mokhtar [33], respectively.

### C. $\alpha + ^{28}\text{Si}$ system

The  $\alpha + ^{28}\text{Si}$  elastic scattering angular distributions at  $E = 104$  and 166 MeV were analyzed using the SFC and SFM

potentials as shown in Fig. 6. It is obvious from Fig. 6 that at 104 MeV the measured data stopped at  $\theta \sim 43^\circ$ . So, data were not available at higher angles close to the rainbow scattering region. We compared our results with the phenomenological optical potential ones [38,43]. We notice from Fig. 6 that the three potentials yielded almost similar fits to data and the corresponding  $\chi^2$  values are comparable.

### D. Volume integrals

The volume integral per interacting nucleon pair for the used  $\alpha$ - $\alpha$  interaction yields a value  $J = -413.5 \text{ MeV fm}^3$ , while for the  $\alpha$ - $n$  interaction  $J = -369.4 \text{ MeV fm}^3$ . Therefore, the obtained real volume integrals for the calculated SFC and SFM potentials have the same energy dependence as expressed by the relations (7)–(10) for  $^{12}\text{C}$  and  $^{16}\text{O}$  targets.

This means that the SFC potential has higher volume integrals than the SFM potential for  $^{12}\text{C}$  target at  $E < 85 \text{ MeV}$  and vice versa for a  $^{16}\text{O}$  target. In the rainbow scattering region SFM potentials have higher  $J_R$  values than SFC potentials for both targets. Our SFM results for carbon nucleus are in a good agreement with those obtained by Smith *et al.* [34] from the phenomenological analysis. Michel *et al.* [4]

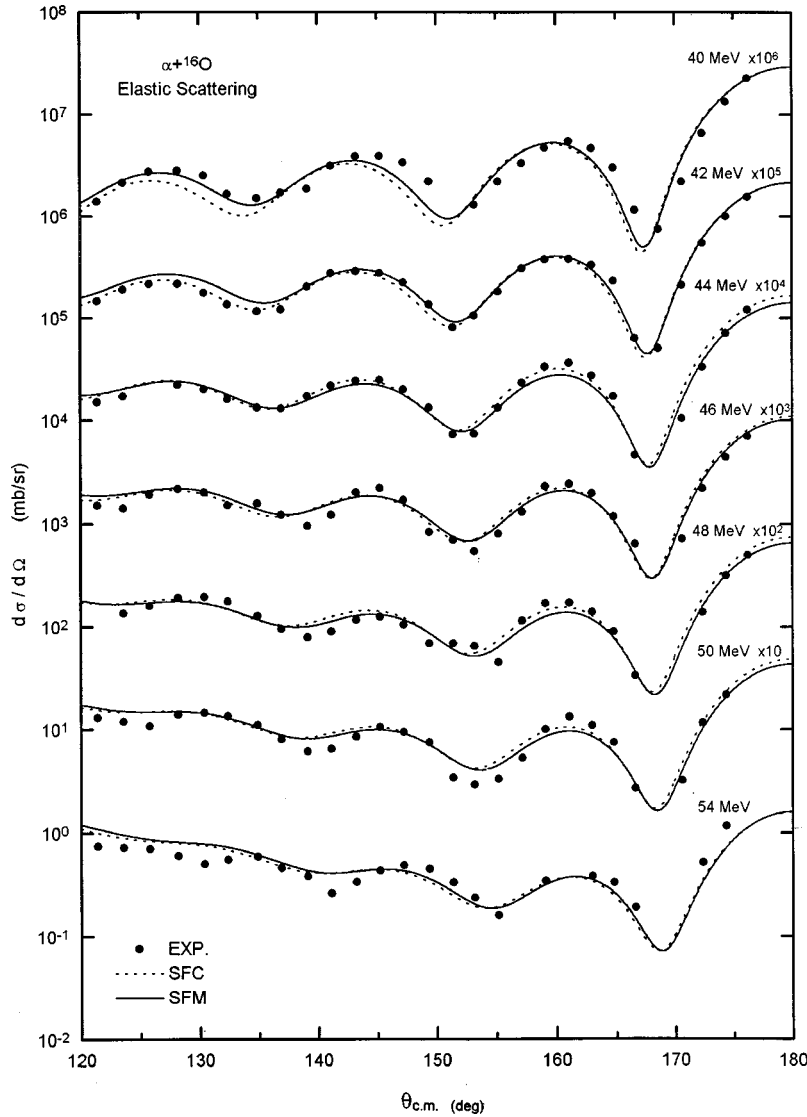


FIG. 5. Same as Fig. 4 but for backward angles at energies of 40–54 MeV [4].

deduced a similar relation from their global phenomenological optical potential for the analysis of  $^{16}\text{O}$  elastic scattering. Our results are consistent with those of Michel *et al.* [4] with a difference  $\sim \pm 10\%$ . Also, our results for  $^{28}\text{Si}$  target are in good agreement with Rebel *et al.* [43] using the phenomenological WS potentials.

For the  $^{12}\text{C}$  target, the imaginary volume integral of both SFC and SFM potentials increases clearly with energy for  $E < 60$  MeV, however, it has a saturation value ( $\sim -100$  MeV fm $^3$ ) for  $E > 100$  MeV. Almost similar behavior can be noticed for the  $^{16}\text{O}$  target. This result obtained for  $^{16}\text{O}$  target coincides exactly with that found by Abele and Staudt [5] using the microscopic potentials based on DDM3Y interaction.

From Tables I and II we notice that both SFC and SFM potentials produce almost similar reaction cross sections with an average difference less than  $\pm 10\%$ . Our results also are in a good agreement with those obtained by some previous investigators [38,43].

To investigate the discrepancy of different forms of the nuclear matter density, we tested the effect of density form on the results of an  $\alpha + ^{16}\text{O}$  system at 48.7 and 54.1 MeV.

We used four different forms for the  $\alpha$ -particle density and two forms for  $^{16}\text{O}$  density. The density parameters used in this investigation are taken from Refs. [13–18]. We used eight different combinations of projectile and target densities. The obtained best fit parameters are almost similar. Also, we noticed that the effect of changing the nuclear density form on the resulting elastic scattering cross sections is almost negligible.

We also analyzed the same data of an  $\alpha + ^{16}\text{O}$  system at 48.7 and 54.1 MeV using a complex SFC potential given by

$$V(R) = (N_r + N_i) V_{\text{SFC}}(R). \quad (11)$$

Our predictions are satisfactory all over the range  $\theta_{\text{c.m.}} = 0^\circ - 180^\circ$  except at the middle region around  $\theta_{\text{c.m.}} = 70^\circ$ . The required real normalization factors are 0.86 and 0.85 while the imaginary ones are 0.17 and 0.18, respectively. We notice that  $N_r$  values are the same as those listed in Table I when we restricted folding procedures to the real part of the potential. In other words, replacing a phenomenological imaginary potential instead of the folded one did not affect the values of the required real renormalization factor.

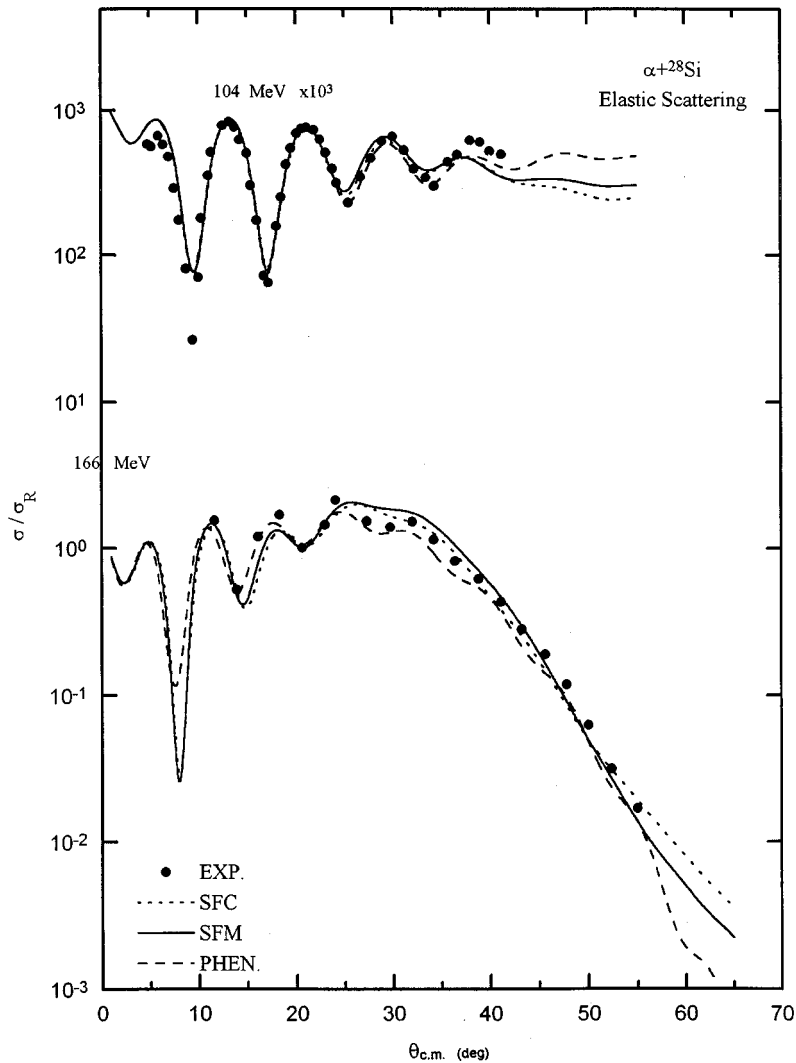


FIG. 6. Same as Fig. 2 but for the  $\alpha+^{28}\text{Si}$  reaction at energies 104 [35] and 166 [39] MeV.

## V. CONCLUSIONS

The derived  $\alpha$ -nucleus SFC potentials based upon an  $\alpha$ - $\alpha$  interaction folded with the  $\alpha$ -cluster distribution functions inside the target nuclei were calculated for the  $^{12}\text{C}$ ,  $^{16}\text{O}$ ,  $^{24}\text{Mg}$ ,  $^{28}\text{Si}$ , and  $^{32}\text{S}$  targets. Three of these interactions,  $\alpha+^{12}\text{C}$ ,  $\alpha+^{16}\text{O}$ , and  $\alpha+^{18}\text{Si}$ , were tested to reproduce the elastic scattering angular distributions. Their predictions were as successful and some times better than those obtained by previous phenomenological and microscopic optical potential analyses. Similar results were obtained using the SFM potentials derived from folding the  $\alpha$ - $n$  interaction with nuclear matter density of the target nuclei.

Although the two  $\alpha$ - $\alpha$  and  $\alpha$ - $n$  interactions were phenomenologically and independently parametrized, they produced almost similar predictions for all the 27 sets of data analyzed in this work.

It was found that SFC and SFM potentials are stronger than the required ones. Therefore, a reducing renormalization coefficient is required for each potential in order to fit ex-

perimental data. This coefficient is weakly energy dependent, where it decreases as energy increases.

Real volume integrals of the SFC and SFM potentials have the same behavior with energy as that of the renormalization factors. However, imaginary volume integrals increase clearly with energy for the ALAS energy region,  $E < 60$  MeV, while a saturation value  $\sim 100$  MeV fm<sup>3</sup> was obtained for  $E > 100$  where rainbow scattering dominates.

The method of restricting the folding procedure to the real part of the potential is satisfactory, since including the folded imaginary part resulted in worse fits in some parts of the angular distributions differential cross sections.

We conclude, also, that the effect of the density form on the calculated differential cross sections is almost negligible.

## ACKNOWLEDGMENTS

The authors wish to thank Professor A. L. Elattar for helpful and interesting comments and Professor R. Smith, U.K., for reading the manuscript.

- [1] Th. Delbar, Gh. Gegoire, G. Paic, R. Ceuleneer, F. Michel, R. Vanderpoorten, A. Budzanowski, H. Dabrowski, L. Freindl, K. Grotowski, S. Micek, R. Planeta, A. Strzalkowski, and K. A. Eberhard, *Phys. Rev. C* **18**, 1237 (1978).
- [2] D. T. Khoa, *Nucl. Phys.* **A484**, 376 (1988).
- [3] H. P. Gubler, U. Kiebele, H. O. Meyer, G. R. Plattner, and I. Sick, *Nucl. Phys.* **A351**, 29 (1981).
- [4] F. Michel, J. Albinski, P. Belery, Th. Delbar, Gh. Gregoire, B. Tasisux, and G. Reidemeister, *Phys. Rev. C* **28**, 1904 (1983).
- [5] H. Abele and G. Staudt, *Phys. Rev. C* **47**, 742 (1993).
- [6] H. Abele, H. J. Hauser, A. Korber, W. Leitner, R. Neu, H. Plappert, T. Rohwer, G. Staudt, M. Straber, S. Welte, M. Walz, P. D. Eversheim, and F. Hinterberger, *Z. Phys. A* **326**, 373 (1987).
- [7] P. E. Hodgson, *Nature (London)* **257**, 446 (1975).
- [8] F. Michel, *Phys. Lett.* **60B**, 229 (1976).
- [9] S. A. E. Khallaf, A. L. Elattar, and M. El-Azab Farid, *J. Phys. G* **8**, 1721 (1982).
- [10] Z. Majka, H. J. Gils, and H. Rebel, *Phys. Rev. C* **25**, 2996 (1982).
- [11] M. El-Azab Farid, *J. Phys. G* **15**, 1437 (1989).
- [12] M. El-Azab Farid, *J. Phys. G* **16**, 461 (1990).
- [13] G. R. Satchler and W. G. Love, *Phys. Rep.* **55**, 183 (1979).
- [14] Y. A. Berezhpny, V. V. Pilipenko, and G. A. Khomenko, *J. Phys. G* **10**, 63 (1984).
- [15] S. Funada, H. Kemeyama, and Y. Sakuragi, *Nucl. Phys.* **A575**, 93 (1994).
- [16] D. Baye, L. Desorgher, D. Guillian, and D. Herschkowitz, *Phys. Rev. C* **54**, 2563 (1996).
- [17] S. Qing-biao, F. Da-chun, and Z. Yi-zhong, *Phys. Rev. C* **43**, 2773 (1991).
- [18] B. Buck, C. B. Dover, and J. P. Vary, *Phys. Rev. C* **11**, 1803 (1975).
- [19] O. M. Knyazkov and E. F. Hefter, *Z. Phys. A* **301**, 277 (1981).
- [20] F. E. Bertrand, G. R. Satchler, D. J. Horen, J. R. Wu, A. D. Bacher, G. T. Emery, W. P. Jones, D. W. Miller, and A. van der Woude, *Phys. Rev. C* **22**, 1832 (1980).
- [21] V. G. Neudatchien, V. I. Kukulin, V. L. Korotkikh, and V. P. Korennoy, *Phys. Lett.* **34B**, 581 (1971).
- [22] B. Buck, H. Friedrich, and C. Wheathly, *Nucl. Phys.* **A275**, 246 (1977).
- [23] L. Marquez, *Phys. Rev. C* **28**, 2525 (1983).
- [24] P. Darriulat, G. Igo, H. G. Pugh, and H. D. Holmgren, *Phys. Rev.* **137**, B135 (1965).
- [25] G. Spitz, H. Klar, and E. W. Schmid, *Z. Phys. A* **322**, 49 (1985).
- [26] N. M. Clarke (unpublished).
- [27] H. Friedrich and K. Langanke, *Phys. Rev. C* **28**, 1385 (1983).
- [28] B. Buck, A. C. Merchant, and S. M. Perez, *Phys. Rev. C* **51**, 559 (1995).
- [29] S. Yamaguchi, K. Yabana, and H. Horiuchi, *Prog. Theor. Phys.* **82**, 217 (1989).
- [30] A. I. Baz, V. Z. Goldberg, N. Z. Darwisch, K. A. Gridnev, V. M. Semjonov, and E. F. Hefter, *Lett. Nuovo Cimento Soc. Ital. Fis.* **18**, 227 (1977).
- [31] G. R. Satchler (private communication).
- [32] N. Baron, R. F. Leonard, and W. M. Stewart, *Phys. Rev. C* **4**, 1159 (1971).
- [33] S. A. E. Khallaf, A. M. Amry, and S. R. Mokhtar, *Phys. Rev. C* **56**, 2093 (1997).
- [34] S. M. Smith, G. Tibell, A. A. Cowley, D. A. Goldberg, H. G. Pugh, W. Reichart, and N. S. Wall, *Nucl. Phys.* **A207**, 273 (1973).
- [35] G. Hauser, R. Lohken, H. Rebel, G. Schatz, G. W. Schweimer, and J. Specht, *Nucl. Phys.* **A128**, 81 (1969).
- [36] F. Carstoiu and M. Lassaut, *Nucl. Phys.* **A597**, 269 (1996).
- [37] D. A. Goldberg, *Phys. Lett.* **55B**, 59 (1975).
- [38] B. Tatischeff and I. Brissaud, *Nucl. Phys.* **A155**, 89 (1970).
- [39] R. Lichtenthaler, A. C. C. Villari, A. Lepine-Szily, and L. C. Gomes, *Phys. Rev. C* **44**, 1152 (1991).
- [40] E. H. Emsel, S. A. H. Abou Steit, M. E. M. Zedan, and M. Y. M. Hassan, *J. Phys. G* **17**, 1755 (1991).
- [41] H. M. Hussein and O. Zohni, *Nucl. Phys.* **A267**, 303 (1976).
- [42] M. El-Azab Farid and G. R. Satchler, *Nucl. Phys.* **A438**, 525 (1985); **A441**, 157 (1985).
- [43] H. Rebel, G. W. Schweimer, G. Schatz, J. Specht, R. Lohken, G. Hauser, D. Habs, and H. Klewe-Nebenius, *Nucl. Phys.* **A182**, 145 (1972).
- [44] M. N. Harakeh, A. R. Arends, M. J. A. De Voigt, A. G. Drentje, S. Y. Van Der Werf, and Van Der Woude, *Nucl. Phys.* **A265**, 189 (1976).